Materialia 4 (2018) 585–594

Contents lists available at ScienceDirect

Materialia

journal homepage: www.elsevier.com/locate/mtla

Full Length Article

Influence of temperature and strain rate on the deformation and damage mechanisms of oxide dispersion strengthened ferritic steels

M. Dadé[a,1], J. Malaplate[a,*], J. Garnier[a], F. Barcelo[a], F. Mompiou[b], P. Wident[a], A. Deschamps[c,d]

[a] DEN-Service de Recherches Métallurgiques Appliquées, CEA, Université Paris-Saclay, F-91191 Gif-Sur-Yvette, France
[b] CEMES, CNRS, Université de Toulouse, 29 rue Jeanne Marvig, 31055 Toulouse, France
[c] Univ. Grenoble Alpes, SIMAP, F-38000 Grenoble, France
[d] CNRS, SIMAP, F-38000 Grenoble, France

ARTICLE INFO

Keywords:
ODS steel
Deformation mechanisms
Tensile tests
Dislocations

ABSTRACT

Deformation and damage mechanisms of Fe-14Cr based oxide dispersion strengthened (ODS) steels have been investigated through a multi scale approach on model materials elaborated by powder metallurgy

Uniaxial tensile behavior was studied from room temperature to 800 °C at several strain rates. Furthermore, the plasticity of Fe-14Cr ODS steels has been analyzed at the grain scale by *in situ* transmission electron microscopy (TEM) straining experiments between room temperature and 650 °C, evidencing a clear evolution with temperature of the dislocation motion. The evolution of yield stress with temperature has been separated into three domains, which can be explained by changes of deformation mechanisms. At low temperatures, the hardening is associated to the pining of dislocations on nano-oxides whereas dislocations motion is thermally activated at higher temperatures. At high temperatures, a competition between intra- and inter-granular mechanisms is observed. The transition in damage mechanism, related to the change of deformation mode, explains the observed reduction of ductility.

1. Introduction

Among materials approached for fuel cladding applications in the next generation of nuclear reactors (GEN IV), Oxide Dispersion Strengthened (ODS) ferritic steels have been particularly studied over the last decade owing to their combination of outstanding mechanical properties at high temperature and their excellent resistance to swelling under irradiation [1–4].

ODS ferritic steels are elaborated using a powder metallurgy process route. A metallic powder is milled with an oxide powder, generally Y_2O_3 and sometimes TiH_2 using a high energy attritor and under a protective atmosphere, which drives a large part of Y, Ti and O in solid solution in the matrix [5]. Then the milled powder must be consolidated, which is usually achieved at high temperature using Hot Extrusion (HE) or Hot Isostatic Pressing (HIP) [4,6]. Besides, several studies of ferritic ODS steels have been carried out on Spark Plasma Sintered (SPS) materials [7,8]. According to a recent *in-situ* characterization [5], oxide nano-clusters, already present in the form of clusters after ball milling, precipitate during the consolidation process.

In a recent paper, the impact of microstructural parameters on the mechanical properties of ODS steels has been evaluated by studying materials where the different components of the microstructure were varied systematically [9]: size and volume fraction of oxide precipitates, grain size, dislocations density. However, this study was limited to macroscopic properties, such as yield stress or creep resistance as a function of temperature. The understanding of the controlling deformation mechanisms as a function of deformation conditions (temperature, strain rate) and complex microstructural features (nanoparticles, high dislocations density, fine grains …) are still largely unclear. Different methods, based on mechanical tests such as stress relaxation, creep or tensile tests, *in situ* straining in a transmission electron microscopy (TEM) [10–13] have been applied to analyze the properties and deformation mechanisms of ODS alloys. Consequently, different mechanisms have been proposed [9,14]. At low temperature, the plastic properties are linked to the combination of dislocation/particles interaction [15,16], grain boundary strengthening [17] and solute solid solution hardening [18]. With increasing temperature, thermally activated mechanisms have been identified: Brandès et al. [12] suggested that creep is controlled by stress assisted-thermal activation. Siska et al. [10] proposed that deformation is governed by dislocation glide/climb mechanisms. Kim et al. [19] found in 14YWT ODS alloys an activation energy between 600 °C and 800 °C close to the activation energy

* Correponding author.
E-mail address: joel.malaplate@cea.fr (J. Malaplate).
[1] Present address: MINES ParisTech, PSL Research University, Centre des Matériaux, CNRS UMR 7633, BP 87, 91003, Evry Cedex, France.

https://doi.org/10.1016/j.mtla.2018.11.016
Received 12 September 2018; Received in revised form 17 November 2018; Accepted 18 November 2018
Available online 19 November 2018

for dislocation climb. Chauhan et al. [15] identified an attractive dislocation/particles interaction (interfacial pinning mechanism where the dislocations are pinned on the departure side of the precipitates), as also previously observed by Artz and Wilkinson [20] or Nardone et al. [21]. The transition temperature for the activation of this mechanism is however not well known. Ramar et al. [22] suggested from volume activation measurements in ODS Eurofer alloy that the transition between weakly thermally activated dislocations/dislocations and dislocations/particles interactions to dislocations climb controlled mechanisms is around 500 °C. Siska et al. [10] suggested a slightly higher temperature (>600 °C) for this transition. Moreover, a contribution of grain boundary sliding to plastic deformation is also evidenced at high temperature, but the temperature above which this effect happens is still not well defined. Praud et al. [16] indicated activity close to grain boundaries around 500 °C. Chauhan et al. [15] and Salmon-Legagneur et al. [23] identified a modification of fracture mechanisms from intragranular to intergranular above 500 °C. The change in fracture mechanisms appears to occur at higher temperature for high Cr ODS steels, e.g., 12Cr-ODS steel [24] and 14Cr-ODS steel [25,26]. Kim et al. [27] also noticed a change of fracture surface morphology between 700 °C and 900 °C to grain boundary decohesion. Sugino et al. [28] identified grain boundary sliding for temperature>900 °C at a strain rate $<10^{-3}$ s^{-1}. At this temperature Masuda et al. [29] also evidenced grain boundary sliding but accommodated by dislocation activity near the grain boundary, possibly leading to continuous dynamic recrystallization.

In this context, the aim of the present study is to elucidate the deformation mechanisms of Fe-14Cr ODS steels at different scales, combining macroscopic properties and the microscopic investigation of plasticity. The influence of microstructural parameters on these deformation mechanisms is studied following on the systematic materials database presented in our former paper [9].

The evolution of ductility, measured both by the total elongation and by the necking coefficient to enable a distinct characterization of damage resistance, is followed as a function of temperature and for two strain rates, and for the variety of microstructures found in these different materials.

The distribution of strain in the different constituents of the microstructure is first followed indirectly by its effect on orientation observed by electron back scattered diffraction (EBSD) in the scanning electron microscope (SEM). At a microscopic level the dislocation motion and their interaction with the oxide nano-particles is studied by *in situ* straining in TEM [16,18].

To evaluate the spatial distribution of deformation, and in particular evaluate the presence of grain boundary sliding [28,29], digital image correlation using focused ion beam (FIB) deposited platinum grids has been carried out on interrupted tensile specimens tested under vacuum.

2. Materials and methods

The alloy compositions and processing details are given in Ref. [9]. Following the same nomenclature the different materials consist of: *US* (unstrengthened), containing no oxide nano-precipitates, *LS* (low strength) containing a low volume fraction of oxide nano-precipitates, *Ref* (reference), containing a medium volume fraction of oxide nano-precipitates, *HS* (High strength), containing a high volume fraction of oxide nano-precipitates, *CP* (coarse precipitates), where precipitates have become coarser due to additional heat treatment as compared to the *Ref* material, with little evolution of grain size, and *Rc* (recrystallized) where cold compression deformation followed by additional heat treatment promotes low temperature recrystallization (and thus a large grain size) with a precipitate size comparable to the *CP* material. Mechanical alloying of a pre-alloyed powder and Y_2O_3 and TiH_2 powders have been used to produce reinforced ferritic steels. The mixture of powders were canned and annealed at 400 or 300 °C, depending of the material, during two hours to reduce the oxygen content. The powders were then subsequently consolidated mainly by Hot Isostatic Pressing (HIP) except for one material (*Rc*) that was consolidated by Hot Extrusion (HE). Tables 1 and 2 summarize respectively the processing details and the main microstructural results of Ref. [9].

Table 1
Summary table of elaboration processing for the different ODS steels.

Material	Elaboration processing
US	Atomized powder + HIP
LS	Ball-milled + HIP
Ref	Ball-milled + HIP
HS	Ball-milled + HIP
CP	Ball-milled + HIP + Heat treatment
Rc	Ball-milled + HIP + cold compression + Heat treatment

EBSD analyses were realized with a Field Emission Gun SEM JEOL JSM-7001FLV apparatus with a voltage of 20 kV. Orientation maps were taken with several acquisition steps. Samples for EBSD were mechanically mirror polished followed by electropolishing during 30 sec at 5 °C with a tension of 27 V in an electrolyte containing 70% of ethanol, 20% of ethylene glycol monobutyl ether and 10% of perchloric acid.

In situ straining TEM investigations were carried out with a JEOL 2010 microscope operating at 200 kV, on micro-tensile specimens (a gauge section of 0.5 mm × 0.9 mm), which were prepared by conventional mechanical polishing down to a thickness smaller than 100 µm. All micro-tensile specimens were electropolished with the same electrolyte as for the EBSD preparation. The polishing voltage for TEM thin specimens was 30 V with an intensity of 170 mA at 5 °C.

Tensile tests were carried out under crosshead displacement control in air at temperature ranging from room temperature to 800 °C in an Instron tensile machine with a load cell of 2 kN and equipped with a radiation furnace. The mean strain rate was applied through a constant crosshead speed. Strain rates of 7.10^{-4} s^{-1} and 1.10^{-5} s^{-1} were used. The specimen temperature was measured by thermocouple. The tensile specimen geometry had a 6 mm gauge length and a 1.5 mm × 0.75 mm rectangular section.

Microscopic measurements of deformation fields by digital image correlation were carried out using Correlmanuv software [30–33] on SEM images based on microgrid deposition at the sample surface. To reduce the high temperature oxidation of ferritic steels, a thin coating of tungsten of about 100 nm was applied using a Gatan Precision Etching Coating Surface (PECS) 682 before the deposition of microgrids. Platinum microgrids (40 × 30 µm with a spacing of 0.75 µm and 95 × 95 µm with a spacing of 5 µm) were deposited on the protected surface with a FIB FEI Helios Nanolab.

3. Results

3.1. Influence of temperature and strain rate on yield stress and fracture strain

Tensile tests have been performed on all materials from room temperature to 800 °C at two strain rates, 7.10^{-4} s^{-1} and 1.10^{-5} s^{-1}. Fig. 1 presents for all alloys the evolution of three parameters: the yield stress (measured at 0.2% plastic strain), the total elongation (expressed in engineering strain in %) and the necking coefficient defined by:

$$Z = \frac{S_0 - S_R}{S_0} \times 100$$

Where S_0 and S_R are respectively the initial and fracture sample sections. Schematically, the difference between the total elongation and the necking coefficient provides an indication of the resistance to damage accumulation after the onset of necking. The influence of strain rate on yield stress is a measurement of the material's strain rate sensitivity (SRS). It was defined using the tensile tests carried out with a strain rate

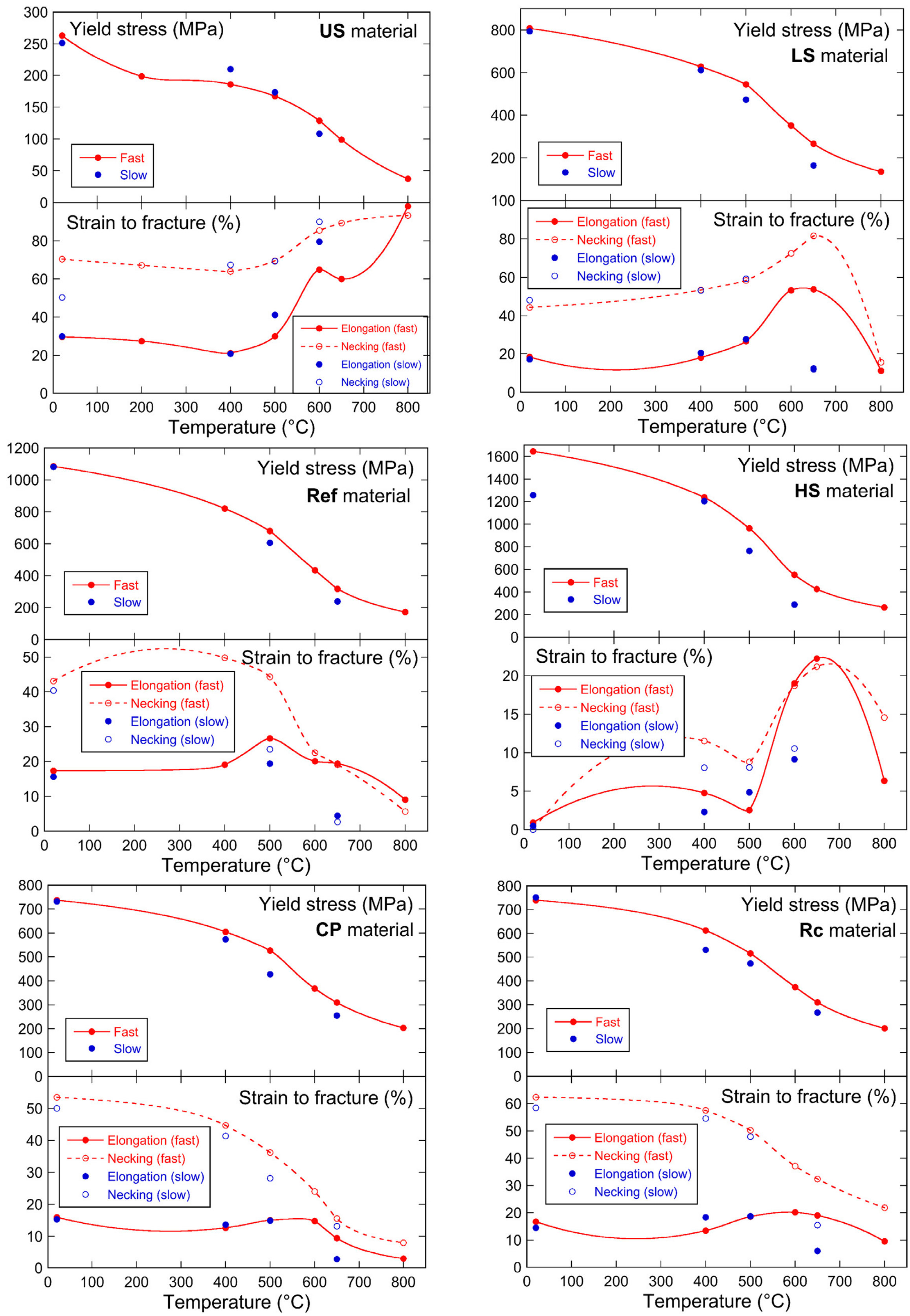

Fig. 1. Evolution with temperature and strain rate of yield stress and ductility parameters for all studied materials.

Table 2
Summary table of microstructural data for the different ODS steels.

	US	LS	Ref	HS	CP	Rc
Mean grain size (μm)	27.6 ± *0.5*	4.3 ± *0.5*	6.5 ± *1.2*	1.8 ± *0.05*	4.5 ± *1.0*	9.5 ± *0.6*
Mean radius (nm)	–	1.56 ± *0.34*	1.27 ± *0.03*	0.9 ± *0.1*	3.1 ± *0.5*	2.55 ± *0.45*
Volume fraction (%)	–	0.31 ± *0.03*	0.52 ± *0.05*	1.03 ± *0.1*	0.53 ± *0.05*	0.62 ± *0.06*
Dislocation density (m^{-2})	$5\ 10^{12} \pm 2\ 10^{12}$	$1\ 10^{14} \pm 4\ 10^{13}$	$9.7\ 10^{13} \pm 3.9\ 10^{13}$	$2.5\ 10^{14} \pm 1\ 10^{14}$	$1\ 10^{13} \pm 4\ 10^{12}$	$5\ 10^{12} \pm 2\ 10^{12}$

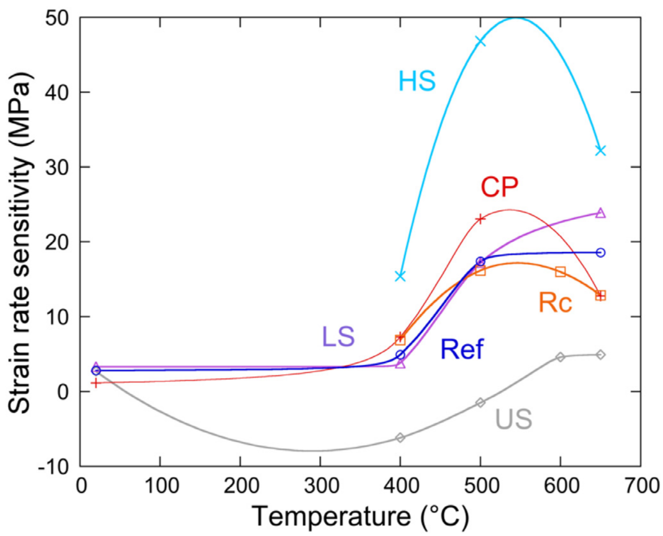

Fig. 2. Evolution with temperature of the strain rate sensitivity for all studied materials.

of 7.10^{-4} and 1.10^{-5} s^{-1}:

$$SRS = \frac{\Delta YS}{\Delta \ln \dot{\varepsilon}}$$

With YS the yield stress and $\dot{\varepsilon}$ the strain rate. The strain rate sensitivity is represented in Fig. 2 for all tested alloys and temperatures.

The *US* material's behavior is representative of a classical stainless steel without the influence of oxide strengthening. This material presents a relatively low yield stress, which further decreases with increasing temperature. The influence of strain rate on this yield stress is non-monotonous. It exhibits a negative value of SRS above room temperature till about 500 °C. As it will be shown later in this paper, it is due to dynamic strain ageing (DSA). Both the total elongation and necking coefficient continuously increase with temperature above 400 °C, reaching of the order of 100% at 800 °C, representative of high temperature plasticity. The difference between total elongation and necking coefficient decreases until these two parameters become equal at 800 °C, illustrating the progressive decrease of damage resistance after necking. There is no significant effect of strain rate on these two fracture parameters.

When adding progressively an increasing fraction of oxide nanoparticles (nano-oxides or NOs) (in the *LS, Ref* and *HS* materials), the behavior is observed to change drastically. As discussed in details in [9], the prime effect of these particles is to increase the yield stress, at all temperatures, and monotonically with respect to the oxide fraction. The effect of strain rate on this yield stress evolution is also different from that of the *US* material: although the low temperature yield stress is insensitive to the strain rate, the SRS increases above 400 °C, to reach a maximum between 500 and 600 °C. This increase of SRS is illustrative of a change in the mechanisms controlling plasticity, presumably linked to the interactions of dislocations with the main obstacles added, namely the oxide nanoparticles. It will be discussed later in this paper in light of the *in situ* tensile tests realized in the transmission electron microscope.

In all these materials, the strength increase brought by the addition of NOs comes together with a dramatic decrease of ductility, both in terms of elongation to fracture or necking coefficient, and this decrease is monotonic with the volume fraction of NOs as well. As already observed before [9], a peak of ductility as well as a peak of necking coefficient is observed around 650 °C, although this is not so obvious for the *Ref* material. Interestingly, a large difference between elongation and necking coefficient is observed in the *LS* material until 650 °C (and then vanishes at 800 °C like in the *US* material), whereas this difference vanishes already at 600 °C for the *Ref* and *HS* materials. This suggests that adding a large fraction of NOs decreases significantly the resistance to post-necking damage of the material, particularly at high temperature, consistently with the decreased overall ductility. Another very interesting feature observed in these results is the influence of strain rate on these ductility parameters. Contrarily to the *US* material, in the NOs-added materials the ductility is observed to drop very significantly in the temperature range 500 and 650 °C when the strain rate is lowered, with commonly a drop of a factor 2 and sometimes more (e.g., *Ref* material, 650 °C). Such a large difference suggests that the damage mechanisms activated in these temperatures range are strongly time-dependent, so that at low strain rate damage accumulates in a smaller strain range and provokes early fracture.

The two last materials, *CP* and *Rc*, present both NOs of larger sizes due to an additional high temperature annealing, with a volume fraction of NOs similar to that of the *Ref* material. The *CP* material has a bimodal grain microstructure similar to that of the *Ref* material, and the *Rc* material is recrystallized with a larger grain size. These two materials present a behavior similar to that of the *Ref* material, with a lower yield stress at lower temperature but similar yield stress at high temperature, and comparable ductility. However, one can observe two interesting differences with the *Ref* material: these two materials keep until 800 °C a significant difference between total elongation and necking coefficient (although smaller as compared to low temperature), and they present a smaller sensitivity of ductility to strain rate. Both these effects suggest that the increased NOs size and / or the modified grain microstructure improved the resistance to damage accumulation.

3.2. Plasticity mechanisms

The above results suggest that at low strain rates, high temperature and in the presence of nano-oxides, damage is localized at the grain boundaries. Such intergranular damage can be easily observed by post-mortem SEM observations on specimens tested with very low strain rate at 650 °C. As illustrated in Fig. 3, corresponding to samples fractured under conditions of creep, in such cases most damage is localized at grain boundaries, especially in nanometer-size regions.

The development of intragranular misorientations after plastic deformation will be now shown, as a first indicator of the extent of intragranular deformation. Fig. 4 shows EBSD maps of longitudinal sections of fractured samples of the *Ref* alloy deformed respectively at room temperature and at 650 °C with a strain rate of 7.10^{-4} s^{-1}. Analyses have been carried out close to the fractured surface. The materials deformed at room temperature and 650 °C present a comparable total deformation (respectively 17–19%).

In both cases, continuous misorientations are observed in the large grains, while the sub-micrometric grains are too small to allow for such observations. These misorientations seem more pronounced at room temperature. They are a good indication that in these deformation conditions a substantial intragranular plastic deformation is taking place.

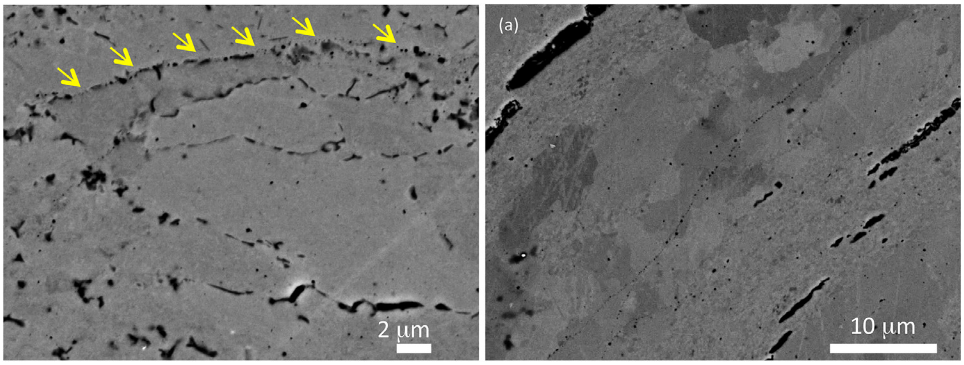

Fig. 3. Observation of damage after deformation to fracture of the *Ref* material at 650 °C under conditions of creep at a stress of 160 MPa (a) and 265 MPa (b) corresponding to a stationary creep strain rates of (a) 6.10^{-9} s^{-1} (a) and (b) 5.10^{-6} s^{-1}.

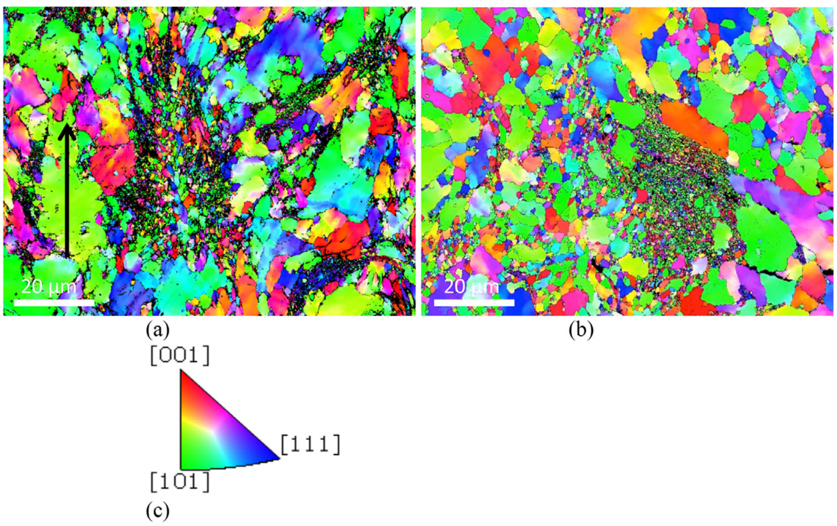

Fig. 4. EBSD orientations map for the *Ref* material deformed at (a) room temperature and (b) 650 °C with a strain rate of 7.10^{-4} s^{-1}. The black arrow on (a) indicates the strain direction. (c) corresponds to the color triangle code.

For the room temperature test, these observations are further confirmed by EBSD analysis realized in a same zone before and after deformation, shown in Fig. 5. A crystallographic orientation effect on the deformation behavior of grains can be noted in these observations. Grains initially oriented in [110], [111] and [001] directions exhibit a very small misorientation. On the contrary, other initial crystallographic orientations, such as [112] which corresponds to purple grains, show more pronounced misorientations.

In order to study the plasticity mechanisms at a microscopic scale, the samples of the *Ref* alloy have been deformed in tension *in situ* in the TEM in the temperature range from room temperature to 650 °C. Fig. 6 show images extracted from a video of an *in situ* TEM tensile test performed at 400 °C. The observed dislocation motion is jerky, illustrated by dislocation pinning—un-pinning by nanoparticles. The dislocation shapes are straight and mostly of screw character. The dislocation motion between pinning points is very quick. Dislocation pile-ups and intra-granular dislocation sources have also been observed in the studied temperature range. At 400 °C, additionally activation of some intra- and inter-granular crack initiations was also noticed.

At higher temperature, a change is observed in the dislocation motion. In some materials, dislocations are observed to move by bursts as illustrated at 450 °C in Fig. 7 in the case of the *US* materials. These dislocation avalanche movements are generally associated to a dynamic strain ageing (DSA) phenomenon, due to the interaction between the moving dislocations and the mobile solutes, generally *C* in Fe-Cr steels [34]. At higher temperature, the movement of dislocations was more continuous. Despite a quick oxidation of the thin TEM specimens, observations have been made up to 650 °C. The viscous motion of dislocations is illustrated at this temperature in Fig. 8. Dislocations are still pinned by precipitates but it is suspected that overcoming is facilitated as thermally activated mechanisms such as dislocation climb should be operative at these high temperatures.

At a larger scale competition between intra- and inter-granular activities is observed. Indeed besides these thermally activated deformation mechanisms, some inter-granular mechanisms such as grain boundaries sliding or decohesion are observed after the *in situ* TEM straining.

3.3. Deformation mapping

In order to monitor the spatial distribution of plasticity, interrupted tensile tests have been carried out on the *Ref* material at two temperatures (room temperature and 650 °C) with a strain rate of 7.10^{-4} s^{-1}. The deformation maps have been acquired by digital image correlation using a platinum microgrid deposited by FIB. To avoid oxidation during the high temperature test, a thin film of tungsten (100 nm) has been coated on the polished surface and the tensile test has been carried out under vacuum.

3.3.1. Deformation at room temperature

The room temperature tensile test has been stopped after 6.6% plastic strain. The platinum microgrid before tensile test is shown in Fig. 9a. The microstructure can be observed below the microgrid. Fig. 9b shows the microstructure obtained after 6.6% of strain. The comparison between the initial state and the deformed specimen highlights significant distorsions of some parts of the microgrid. As illustrated by the red circles in Fig. 9, these main microgrid distortions are located inside large grains because of their comparatively lower strength compared to the nano-grains, mainly related to a grain size effect since TEM observations did not show an appreciable difference of precipitate size between the different grain families. Some very limited inter-granular deformations

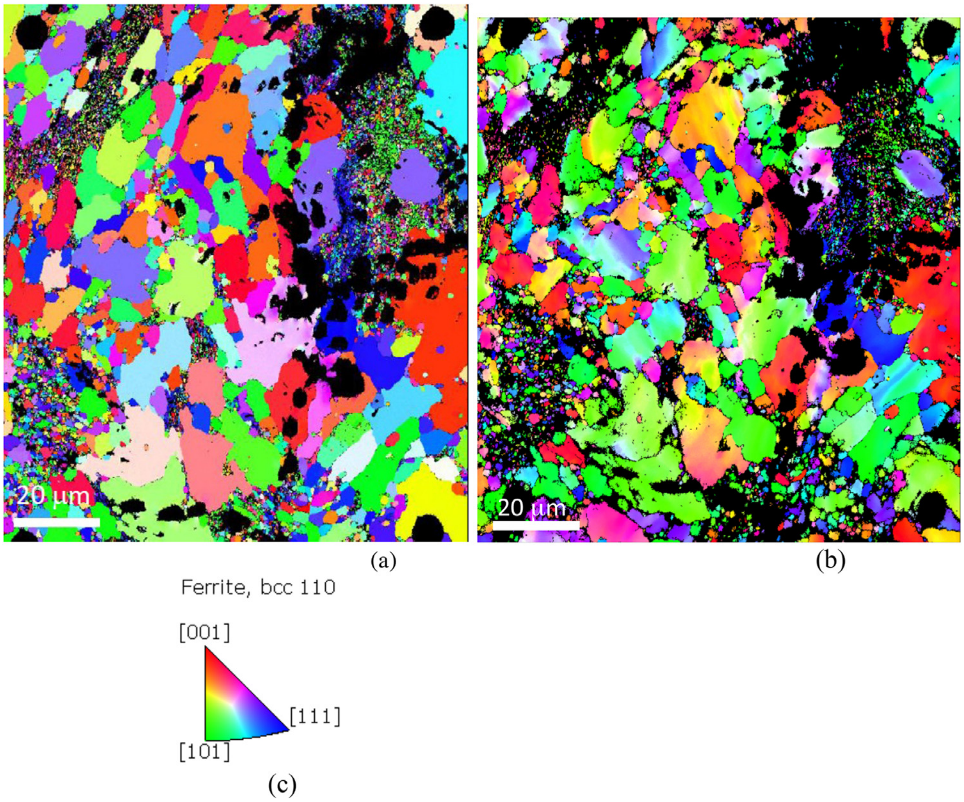

Fig. 5. EBSD analyses of the *Ref* material (a) before deformation and (b) after deformation to fracture at room temperature with a strain rate of 7.10^{-4} s^{-1}. (c) color triangle code.

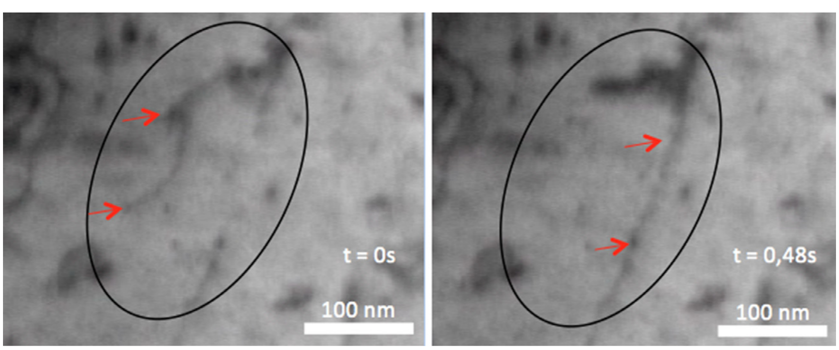

Fig. 6. TEM video captures during *in-situ* deformation of the *Ref* material at 400 °C. Jerky dislocation motion by successive steps of un-pinning and pinning on the nanoparticles. The red arrows correspond to pinning points (For interpretation of the references to color in this figure legend, the reader is referred to the web version of this article).

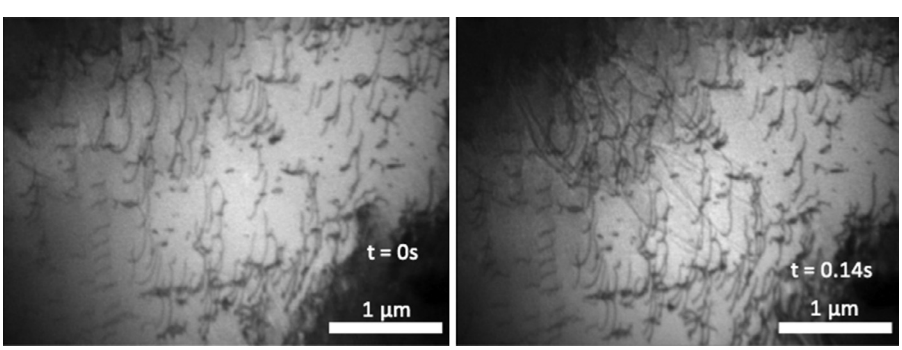

Fig. 7. TEM video captures during *in-situ* deformation of the *US* material at 450 °C. Dislocations appear to move as bursts in a collective manner.

can also be suspected (blue circles). These observations confirm, consistently with the EBSD maps shown above, that the room temperature deformation mechanisms are predominantly intra-granular.

3.3.2. Deformation at high temperature

The 650 °C tensile test has been carried out on the *Ref* material in a secondary vacuum furnace up to a strain of about 7.2%.

The SEM picture of Fig. 10a shows the platinum microgrid after deformation. The protective coating presents a number of cracks, however digital image correlation (DIC) was still possible. Fig. 10b shows the deformation map obtained by DIC (uniaxial deformation ε_{11}) superposed with the EBSD analysis of the undeformed specimen. The first observation is that a small difference of deformation between small and large grains can be noted. Regions of sub-micrometer grains are the regions showing the smallest amount of plastic strain. On the contrary, an im-

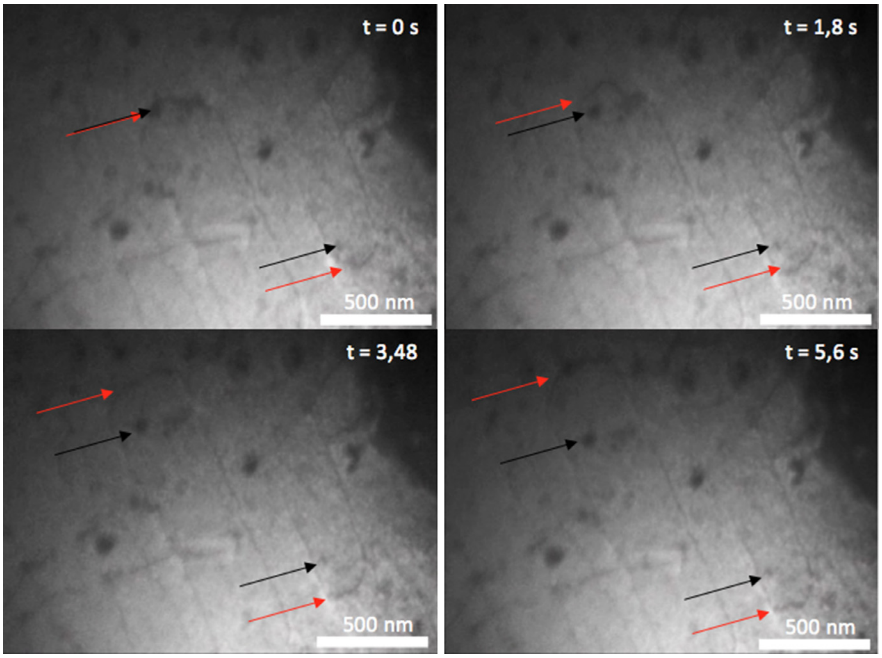

Fig. 8. TEM video captures during *in-situ* deformation of the *Ref* material at 650 °C, illustrating the continuous dislocation motion at high temperature. The red arrows show the movement of the dislocations compared to fixed points designed by black arrows. (For interpretation of the references to color in this figure legend, the reader is referred to the web version of this article).

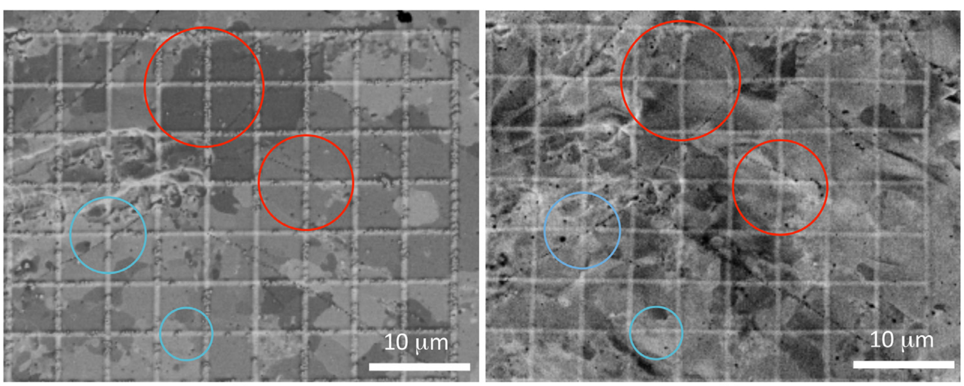

Fig. 9. SEM images of the *Ref* material (a) initial microstructure (b) after 6.62% of strain at room temperature with a strain rate of 7.10^{-4} s^{-1}. Red and blue circles correspond respectively to intra-granular and inter-granular deformations evidenced by microgrid distorsions. (For interpretation of the references to color in this figure legend, the reader is referred to the web version of this article).

portant concentration of deformation is observed in the same regions where cracking of the protective layer has occurred, and these regions are correlated with the presence of boundaries between large grains.

4. Discussion

4.1. Evolution of deformation mechanisms of ODS steels with temperature

Taking into account the results of the recent study of mechanical properties evolution on a large temperature range of ODS ferritic steels exposed in [9], three domains can be distinguished on the evolution of yield stress with temperature:

- A low temperature regime (room temperature to 400 °C), presenting an athermal plateau where the evolution of yield stress is mainly controlled by that of the elastic modulus;
- An intermediate temperature domain (400 °C–600 °C) with a significant drop of yield stress
- A high temperature regime (above 600 °C) where the decrease of yield stress becomes more moderate.

4.1.1. Deformation mechanisms at low temperature

Our EBSD observations on deformed samples show that the plasticity of Fe-14Cr ODS steels at low temperature is mainly controlled by intra-granular mechanisms, illustrated by the development of intra-granular misorientations. Our results are in good agreement with the *in situ* SEM tensile test carried out by Boulnat [35]. In these two cases, EBSD analyses show changing of crystallographic orientation of large grains, from [111] (blue grains) [35] and/or [112] (purple grains) towards [110] direction. According to Kocks et al. [36], an α fiber (<110> direction) is classically observed in bcc materials after tensile tests or hot extrusion. Boulnat suspected a rotation of nanometric grains along grain boundaries after straining at room temperature [35], however the comparison of EBSD picture before and after tensile test (Fig. 5) does not confirm this observation whereas intragranular deformations into large grains have been highlighted both by Boulnat [35] and in this work.

At microscopic scale, our *in situ* TEM straining experiments confirm the observations of Praud et al. [16] showing screw dislocations with jerky movements and a straight-line shape between room temperature and 400 °C. A high pinning force of nano-oxides, together with a relatively low friction stress [9,37], explains these observations. Nanoparticles radius being of the order of 1 nm, it is difficult to conclude from the TEM observations if nanoparticles are overcome by a by-passing or a shearing mechanism. However, recent modelling of the yield stress contributions in these materials showed that the stress could be adequately modelled by a by-passing mechanism [9]. Moreover, intra-

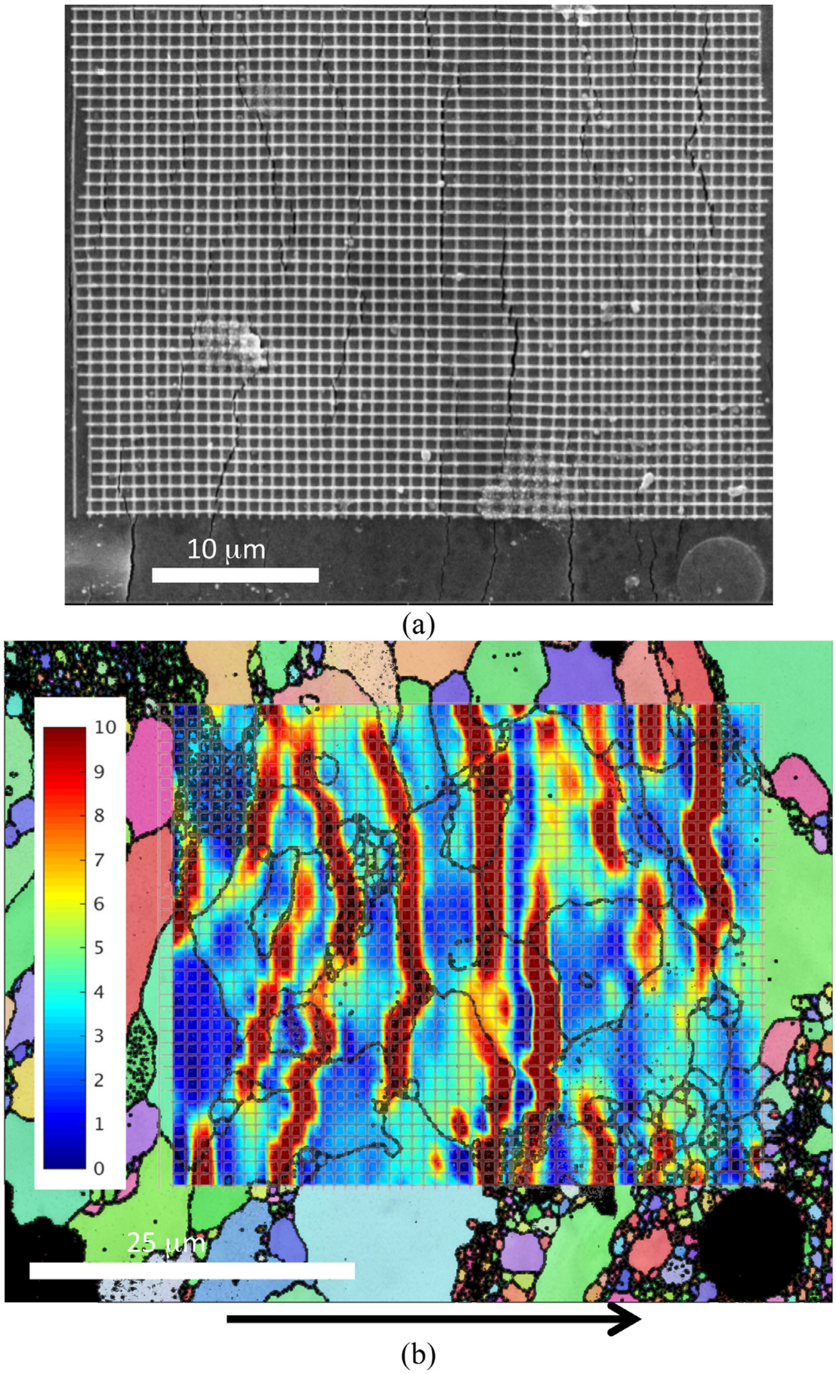

Fig. 10. (a) Image of the microgrid after a tensile test to failure of the *Ref* material at 650 °C with a strain rate of 7.10^{-4} s^{-1} and (b) superposition of the deformation map obtained by image correlation on the orientation map obtained by EBSD. The black arrow indicates the strain direction.

granular sources of dislocations have been observed at low temperature as in Ref. [38].

4.1.2. Deformation mechanisms at intermediate and high temperatures

Several deformation mechanisms have been observed above 400 °C up to about 650 °C. Dislocation motion is still jerky with individual movements of dislocations and some crack initiation appear at temperatures close to 400 °C. With the increase of temperature the dislocation motion evolved more or less progressively to a more viscous displacement at high temperature: individual dislocations thus move continuously exhibiting curved shapes. In this range of temperature dislocations are still pinned by nanoparticles, however thermally activated mechanisms, such as climb/glide of dislocations, are predicted to become easy in these high temperature conditions [9,10,16]: the crossing should thus be easier. In some materials, as illustrated on the un-strengthened material, a supplementary step is observed as a transition between low temperature and high temperature domain. In this intermediate range, dislocations always move jerkily but in a collective manner, by the displacement of dislocation bursts. This type of motion corresponds to a domain of dynamic strain-ageing (DSA). Caillard and Bonneville [34,39] have observed similar mechanisms on Fe-Cr based steels at close temperature range (from 200 °C to 500 °C). DSA is usually associated to serrations on the tensile curves (Portevin – Le Chatelier phenomenon) but no signs of them have been seen during our tests as shown in our former paper [9]. According to Wang [40], the DSA temperature range can be larger than that of Portevin – Le Chatelier effect. The DSA phenomenon in the *US* material is consistent with the negative strain rate sensitivity present in this temperature range (see Fig. 2).

In the oxide-reinforced materials, the dislocation—nano-oxide interaction can modify the strain rate sensitivity, which is the main parameter involved in the DSA effect. In fact, the measurement of strain rate sensitivity shows that it increases in this temperature range to reach a peak around 600 °C (see Fig. 2). This strain rate sensitivity is therefore not related to the matrix displacement of dislocations but most probably to the progressive activation of climb-assisted precipitate by-passing, which has been shown to control the evolution of yield stress [9].

Moreover, even if intra-granular deformation mechanisms are still present at temperatures above 600 °C as shown by the *post-mortem* EBSD observations, it comes along with a very significant inter-granular deformation activity, as shown by the tensile test with platinum microgrid tracking and images correlation. Accordingly, *in situ* TEM observations highlighted decohesion at grain boundaries. According to Sugino et al. [28,41] and Masuda et al. [29] investigations of deformation mechanisms, grain boundaries sliding can be evidenced at ~900 °C, depending notably on the strain rate conditions. According to [16], inter-granular sources have been noted on similar ODS ferritic steels consolidated by hot extrusion, already at 500 °C. Chauhan et al. [15] also noticed a more intense dislocation activity close to grain boundaries, as dislocations pile up at higher temperature (550 °C and more).

4.2. Evolution of elongation and necking coefficient

Two parameters can describe ductility: the total elongation, which is mainly controlled by the pre-necking plasticity, and the necking coefficient, representative of the local deformation to fracture, and therefore of the ability of the material to resist ductile fracture.

At low temperature (until 400 °C), all oxide-reinforced materials present a weakly strain rate dependent ductility, and a large difference between the total elongation and the necking coefficient (except for the brittle *HS* material tested at room temperature). The first feature is well in agreement with plasticity occurring mainly inside the grains and being controlled by dislocation-precipitate and dislocation-dislocation interactions, with a high associated activation volume. The second feature is representative of a good resistance to ductile fracture.

At 500 °C and above, the characteristics of ductility drastically change. Overall the ductility increases at the high strain rate, resulting in the well-known elongation peak around 600 °C [16,28]. This increase comes together with a higher SRS, which seems at first inconsistent with the observation of DSA in the same temperature range. However, the activation of climb-assisted precipitate by-passing, which is a strongly rate dependent mechanism, can explain this increase of SRS and associated ductility increase. The situation is very different at slow strain rate. In this case, the elongation continuously decreases in most materials (except the *HS* material, however its elongation peak is still much less pronounced), and a large difference is observed between the elongations measured at the two strain rates. Moreover, the difference between total elongation and necking coefficient cancels out, showing the appearance of a low resistance to ductile damage. Our observations of the mechanisms of plasticity suggest an increasing role of grain boundary plasticity in this temperature range. Such grain boundary activity such as grain boundary sliding, is strongly rate dependent and is expected to play a much more prominent role at low strain rates. In the framework of this interpretation it can be expected that the microstructure at the grain boundaries plays an important role on this mechanism. It is therefore interesting to compare the *Ref, CP* and *Rc* materials whose microstructures differ markedly in this respect, whereas the volume fraction of strengthening particles is identical (and the strength in this temperature range is comparable). At low strain rate, the *Ref* and *CP* materials show a very low ductility (2 to 3%). However, the *Rc* material almost doubles this ductility and still shows a necking coefficient of the order of 15%. It seems, therefore, that changing the grain microstructure is an effective way to improve the low strain rate ductility. This effect could be due to the absence of sub-micrometer grains in this material, the low dislocation density, or to the change in the location of the grain boundaries away from the impurities and large particles inherited from the powder metallurgy process.

In line with the cross-section observations of damage presented in Fig. 3, all the data presented here is consistent with the activation in the temperature range 500–650 °C of grain boundary strain localization, probably including grain boundary sliding, strongly strain rate dependent, which results in rapid grain boundary damage and promotes a low ductility at low strain rates. Intra-granular mechanisms, such as by passing of nano-oxides, are still activated (Fig. 8), however inter-granular mechanisms are greater at low strain rates. At higher strain rates this inter-granular mechanism is less active and a ductility peak appears due to improved strain rate sensitivity, as it has been shown before by Steckmeyer el al. [25].

No tests were realized at 800 °C, low strain rate in the present study. However, already at the higher strain rate, all ductility parameters experience a sharp drop, without a major change in SRS. Most probably, at such high temperatures grain boundary strain localization becomes active at all strain rates and promotes a high rate of damage accumulation.

5. Conclusions

In this present work, the deformation and damage mechanisms of ODS ferritic steels consolidated by hot isostatic pressing have been investigated from room temperature to 650 °C. *Ex situ* and *in situ* experiments have been carried out at different temperatures. The main conclusions are:

- The dominant deformation mechanisms show a transition from intra-granular to inter-granular, which depends both on temperature and strain rate.
- At high strain rate ductility improves with temperature and shows a maximum around 600 °C, due to an increase of strain rate sensitivity due to the activation of climb-controlled by-passing of the nano-oxide particles by dislocations.
- At low strain rate, the activation of inter-granular plastic localization results in early damage accumulation and low ductility. Recrystallization seems to be an effective way to limit the detrimental effect of this mechanism, depending on the thermo-mechanical treatment [42].

Acknowledgements

The authors would like to acknowledge Daniel Caillard (CEMES Toulouse) for the fruitful discussions, Louis Ziolek (CEA Saclay) and Jean Luc Flament (CEA Saclay) for mechanical tests under vacuum, Benoit Arnal (CEA Saclay) for his help on the depositing of platinum microgrids and Didier Bossu (CEA Saclay) for the protective coating tests. The *in situ* TEM straining experiments were carried out thanks to METSA program. The authors would like to acknowledge the LTMEx for materials supplying. This work was supported by the French government, managed by the French National Research Agency, under the "Investissements d'avenir" program bearing the reference number ANR-11-EQPX-0020. This work has been supported by the French National Research Agency under the "Investissement d'Avenir" program reference No. ANR-10-EQPX-38-01. This work was supported by the Nuclear Energy Division of the French Commission for Atomic Energy and alternative energies (CEA) in the context of the MACNA framework agreement.

Declaration of interest

The authors declare that they have no known competing financial interests or personal relationships that could have appeared to influence the work reported in this paper.

References

[1] M.B. Toloczko, D.S. Gelles, F.A. Garnier, R.J. Kurtz, K. Abe, Irradiation creep of various ferritic alloys irradiated at ∽400°C in the PFR and FFTF reactors, J. Nucl. Mater. 329–333 (2004) 352.

[2] R.L. Klueh, Elevated temperature ferritic and martensitic steels and their application to future nuclear reactors, Int. Mate. Rev. 50 (2005) 287.

[3] P. Yvon, F. Carré, Structural materials challenges for advanced reactor systems, J. Nucl. Mater. 385 (2009) 217.

[4] P. Dubuisson, Y. De Carlan, V. Garat, M. Blat, ODS Ferritic/martensitic alloys for Sodium Fast Reactor fuel pin cladding, J. Nucl. Mater. 428 (2012) 6.

[5] A. Deschamps, F. De Geuser, J. Malaplate, D. Sornin, When do oxide precipitates form during consolidation of oxide dispersion strengthened steels, J. Nucl. Mater. 482 (2016) 83.

[6] I. Hilger, X. Boulnat, J. Hoffmann, C. Testani, F. Bergner, Y. De Carlan, F. Ferraro, A. Ulbricht, Fabrication and characterization of oxide dispersion strengthened (ODS) 14Cr steels consolidated by means of hot isostatic pressing, hot extrusion and spark plasma sintering, J. Nucl. Mater. 472 (2016) 206.

[7] Q. Sun, T. Zhang, X. Wang, Q. Fang, T. Hao, C. Liu, Microstructure and mechanical properties of oxide dispersion strengthened ferritic steel prepared by a novel route, J. Nucl. Mater. 424 (2012) 279.

[8] X. Boulnat, D. Fabrègue, M. Perez, Y. De Carlan, M.H. Mathon, High-Temperature Tensile Properties of Nano-Oxide Dispersion Strengthened Ferritic Steels Produced by Mechanical Alloying and Spark Plasma Sintering, Metal. Mater. Trans. A 44 (2013) 2461.

[9] M. Dadé, J. Malaplate, J. Garnier, F. De Geuser, F. Barcelo, P. Wident, A. Deschamps, Influence of microstructural parameters on the mechanical properties of oxide dispersion strengthened Fe-14Cr steels, Acta Mater. 127 (2017) 165.

[10] F. Siska, L. Stratil, H. Hadraba, S. Fintova, I. Kubena, T. Zalezak, D. Bartkova, High temperature deformation mechanisms in the 14% Cr ODS alloy, Mater. Sci. Eng. A 689 (2017) 34.

[11] J.H. Kim, T.S. Byun, D.T. Hoelzer, S.W. Kim, B.H. Lee, Temperature dependence of strengthening mechanisms in the nanostructured ferritic alloy 14YWT: Part I—Mechanical and microstructural observations, Mater. Sci. Eng. A 559 (2013) 101.

[12] M.C. Brandes, L. Kovarik, M.K. Miller, G.S. Daehn, M.J. Mills, Creep behavior and deformation mechanisms in a nanocluster strengthened ferritic steel, Acta Mater 60 (2012) 1827.

[13] D. Häussler, B. Reppich, M. Bartsch, U. Messerschmidt, Interaction processes between dislocations and particles in the ODS nickel-base superalloy INCONEL MA 754 studied by means of in situ straining in an HVEM, Mater. Sci. Eng. A 309 (2001) 500.

[14] A. Chauhan, F. Bergner, A. Etienne, J. Aktaa, Y. De Carlan, C. Heintze, D. Litvinov, M. Hernandez-Mayoral, E. Oñorbe, B. Radiguet, A. Ulbricht, Microstructure characterization and strengthening mechanisms of oxide dispersion strengthened (ODS) Fe-9%Cr and Fe-14%Cr extruded bars, J. Nucl. Mater. 495 (2017) 6.

[15] A. Chauhan, D. Litvinov, Y. de Carlan, J. Aktaa, Study of the deformation and damage mechanisms of a 9Cr-ODS steel: Microstructure evolution and fracture characteristics, Mater. Sci. Eng. A 658 (2016) 123.

[16] M. Praud, F. Mompiou, J. Malaplate, D. Caillard, J. Garnier, A. Steckmeyer, B. Fournier, Study of the deformation mechanisms in a Fe-14% Cr ODS alloy, J. Nucl. Mater. 428 (2012) 90.

[17] J.H. Kim, T.S. Byun, D.T. Hoelzer, S.W. Kim, B.H. Lee, Temperature dependence of strengthening mechanisms in the nanostructured ferritic alloy 14YWT: Part II—Mechanistic models and predictions, Mater. Sci. Eng. A 559 (2013) 111.

[18] A. Wasilkowska, M. Bartsch, U. Messerschmidt, R. Herzog, A. Czyrska-Filemonowicz, Creep mechanisms of ferritic oxide dispersion strengthened alloys, J. Mater. Process. Technol. 133 (2003) 218.

[19] J.H. Kim, T.S. Byun, D.T. Hoelzer, Stress relaxation behavior of nanocluster-strengthened ferritic alloy at high temperatures, J. Nucl. Mater. 425 (2012) 147.

[20] E. Arzt, D.S. Wilkinson, Threshold stresses for dislocation climb over hard particles: The effect of an attractive interaction, Acta Metall 34 (1986) 1893.

[21] V.C. Nardone, D.E. Matejczyk, J.K. Tien, The threshold stress and departure side pinning of dislocations by dispersoids, Acta Metall 32 (1984) 1509.

[22] A. Ramar, P. Spätig, R. Schäublin, Analysis of high temperature deformation mechanism in ODS EUROFER97 alloy, J. Nucl. Mater. 382 (2008) 210.

[23] H. Salmon-Legagneur, S. Vincent, J. Garnier, A.F. Gourgues-Lorenzon, E. Andrieu, Anisotropic intergranular damage development and fracture in a 14Cr ferritic ODS steel under high-temperature tension and creep, Mater. Sci. Eng. A 722 (2018) 231.

[24] A. Chauhan, D. Litvinov, J. Aktaa, High temperature tensile properties and fracture characteristics of bimodal 12Cr-ODS steel, J. Nucl. Mater. 468 (2016) 1.

[25] A. Steckmeyer, M. Praud, B. Fournier, J. Malaplate, J. Garnier, J.L. Béchade, I. Tournié, A. Bougault, P. Bonnaillie, Tensile properties and deformation mechanisms of a 14Cr ODS ferritic steel, J. Nucl. Mater. 405 (2010) 95.

[26] J.H. Kim, T.S. Byun, D.T. Hoelzer, Tensile fracture characteristics of nanostructured ferritic alloy 14YWT, J. Nucl. Mater. 407 (2010) 143.

[27] J.H. Kim, T.S. Byun, D.T. Hoelzer, High temperature deformation mechanisms of nano-structured ferritic alloys in the context of internal variable theory of inelastic deformation, J. Nucl. Mater. 442 (2013) 458.

[28] Y. Sugino, S. Ukai, B. Leng, N. Oono, S. Hayashi, T. Kaito, S. Ohtsuka, Grain boundary sliding at high temperature deformation in cold-rolled ODS ferritic steels, J. Nucl. Mater. 452 (2014) 628.

[29] H. Masuda, S. Taniguchi, E. Sato, Y. Sugino, S. Ukai, Two-Dimensional Observation of Grain Boundary Sliding of ODS Ferritic Steel in High Temperature Tension, Mater. Trans. 55 (2014) 1599.

[30] G. Martin, D. Caldemaison, M. Bonert, C. Pinna, Y. Bréchet, M. Véron, J.D. Mithieux, T. Pardoen, Characterization of the high temperature strain partitioning in duplex steels, Exp. Mech. 53 (2012) 205.

[31] E. Héripré, M. Dexet, J. Crépin, L. Gélébart, A. Roos, M. Bornert, D. Caldemaison, Coupling between experimental measurements and polycrystal finite element calculations for micromechanical study of metallic materials, Int. J. Plast. 23 (2007) 1512.

[32] L. Allais, M. Bornert, T. Bretheau, D. Caldemaison, Experimental characterization of the local strain field in a heterogeneous elastoplastic material, Acta Metal. Mater. 42 (1994) 3865.

[33] A. Lechartier, G. Martin, S. Comby, F. Roussel-Dherbey, A. Deschamps, M. Mantel, N. Meyer, M. Verdier, M. Veron, Influence of the Martensitic Transformation on the Microscale Plastic Strain Heterogeneities in a Duplex Stainless Steel, Metal Mater Trans A 48 (2017) 20.

[34] D. Caillard, Dynamic strain ageing in iron alloys: The shielding effect of carbon, Acta Mater 112 (2016) 273.

[35] X. Boulnat, FAST high-temperature consolidation of Oxide-Dispersion Strengthened (ODS) steels : Process, microstructure, precipitation, properties, PhD thesis, INSA Lyon, 2012.

[36] U.F. Kocks, C.N. Tomé, H.R. Wenk, Texture and Anisotropy, Cambridge University Press, 2000.

[37] D. Caillard, Kinetics of dislocations in pure Fe. Part I. In situ straining experiments at room temperature, Acta Mater 58 (2010) 3493.

[38] J. Malaplate, F. Mompiou, J.L. Béchade, T. Van Den Berghe, M. Ratti, Creep behavior of ODS materials: A study of dislocations/precipitates interactions, J. Nucl. Mater. 417 (2011) 205.

[39] D. Caillard, J. Bonneville, Dynamic strain aging caused by a new Peierls mechanism at high-temperature in iron, Scripta Mater 95 (2015) 15.

[40] H. Wang, Comportement mécanique et rupture des aciers au C-Mn en présence de vieillissement dynamique, PhD Thesis, Ecole Centrale Paris, 2011.

[41] Y. Sugino, S. Ukai, N. Oono, S. Hayashi, T. Kaito, S. Ohtsuka, H. Masuda, S. Taniguchi, E. Sato, High temperature deformation mechanism of 15CrODS ferritic steels at cold-rolled and recrystallized conditions, J. Nucl. Mater. 466 (2015) 653.

[42] M. Dadé, J. Malaplate, J. Garnier, F. De Geuser, N. Lochet, A. Deschamps, Influence of consolidation methods on the recrystallization kinetics of a Fe-14Cr based ODS steel, J. Nucl. Mater. 472 (2016) 143.